Measurement of Magnetic Nanoparticles Using High Transition Temperature Superconducting Quantum Interference Devices

Ji Wang, Hao Li, Ethan Y. Cho, Jay C. LeFebvere, and Shane A. Cybart

Abstract—Superconducting quantum interference device (SQUID) based sensors hold promise for magnetic detection of magnetically tagged biological cells. In this work, a high transition temperature (high- $T_{\rm C}$) direct-coupled SQUID micro-magnetometer was fabricated from a 30-nm-thick YBa₂ Cu₃O_{7- δ} (YBCO) thin film. The SQUID was directly written with irradiation from a finely focused helium ion beam without milling or etching any material. An experiment estimating the sensitivity of the magnetometer to magnetic nanoparticles was conducted that revealed the magnetic moment calculated based on the measurement of the SQUID magnetometer is consistent to that obtained from susceptibility measurements.

Index Terms—SQUID, nanoparticles, magnetometer.

I. Introduction

AGNETIC nanoparticles are playing an increasingly important role in medicine for cellular tagging [1], cell sorting [2], [3] and image contrasting[4]–[6]. As nanoparticles synthesis and cellular tagging methods mature, there is an important need for more sensitive detection electronics with higher detection resolution at the single cell level. Superconducting quantum interference devices (SQUIDs) are well suited for these applications because of their high sensitivity to magnetic flux. However, the requirement of cooling the sensors below the superconducting critical temperature complicates engineering SQUID based systems. Nearly all commercial SQUID sensors are made of conventional metal low transition temperature (low- T_C) superconductors operating at the temperature of the boiling

Manuscript received October 31, 2018; accepted February 7, 2019. Date of publication March 12, 2019; date of current version April 2, 2019. This work was supported by AFOSR Grant No. FA955015-1-0218, ARO Grant W911NF1710504, NSF Grant No. 1664446, NIH Contract No. j1R43EB023147-01, and UCOP MRPI Award No. 009556-002. (Corresponding author: Shane A. Cybart.)

- J. Wang, H. Li, and E. Y. Cho are with the Department of Mechanical Engineering, University of California, Riverside, Riverside, CA 92521 USA (e-mail: jwang341@ucr.edu; haoli@ucr.edu; eycho@ucr.edu).
- J. C. LeFebvere is with the Department of Physics, University of California, Riverside, Riverside, CA 92521 USA (e-mail: jlefe001@ucr.edu).
- S. A. Cybart is with the Department of Mechanical Engineering, University of California, Riverside, Riverside, CA 92521 USA, and also with the Material Science and Engineering Program University of California, Riverside, Riverside, CA 92521 USA (e-mail: cybart@ucr.edu).

Color versions of one or more of the figures in this paper are available online at http://ieeexplore.ieee.org.

Digital Object Identifier 10.1109/TASC.2019.2904479

point of liquid helium 4.2 K. Challenges arise from the large temperature gradient between room temperature biological specimens and the senors at 4.2 K. Not only does the sensor require a great deal of cooling power it also requires several millimeters of insulation or vacuum in between which severely limits the resolution. High transition temperature superconductor (high- $T_{\rm C}$) SQUIDs operating on single stage cryocoolers at elevated temperatures could significantly decrease the complexity, cost, power, and weight of bio-medical SQUID systems. More important, higher temperature will relax insulation requirements allowing for the SQUID sensors to be located closer to the specimen. The most prominent high- $T_{\rm C}$ superconductor, YBa₂ Cu₃ $O_{7-\delta}$ (YBCO) is a ceramic transition metal oxide material with a high transition temperature of 92 K [7], crystallizing in a complex distorted perovskite orthorhombic structure. As a result, the electrical properties of YBCO are highly anisotropic. The conductivity and the superconducting coherence length in the a-b plane are approximately an order of magnitude higher than the values along the c-axis [8], [9]. The aforementioned properties severely complicate high- $T_{\rm C}$ Josephson junction fabrication because small nanoscale features are required for the Josephson tunnel barrier. Furthermore, unlike conventional metals, YBCO is very difficult to grow, pattern and etch. This severely restricts and complicates multi-layer YBCO circuits such as superconducting transformers for flux concentration into the sensor. These issues are exasperated when scaling YBCO sensors to cellular micrometer dimensions. Several fabrication techniques have been utilized in the past for high- $T_{\rm C}$ SQUIDs such as grain boundary [10], ramp-edge [11], step edge [12] and ion irradiation [13], [14].

In recent work by Cho *et al.* [15], a novel approach to YBCO direct-coupled micro-SQUID magnetometer fabrication was reported utilizing a helium ion microscope (HIM) [16]. In this work, the focused ion beam of the HIM was used to write insulating features into the plane of a single YBCO thin film to define both Josephson junctions [17] and a nano-slit SQUID loop. Irradiation from the HIM disorders the YBCO and as a result, the critical temperature is reduced in a controllable way with increasing ion irradiation dose. For moderate doses of the order of 10^{16} He⁺/cm² the material is rendered insulating and it no longer superconducts. Ion irradiated devices have been shown to be remarkably stable for several years after fabrication [18].

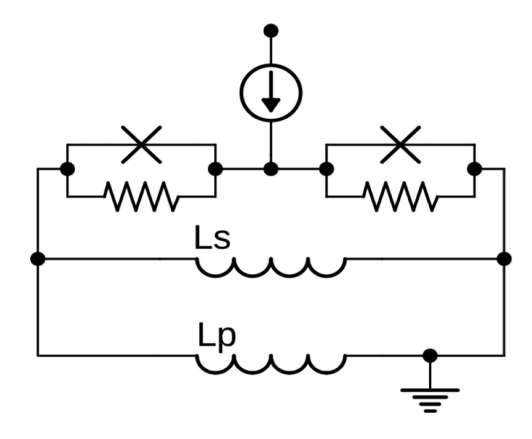


Fig. 1. Schematic of the magnetometer. A pick-up loop with self-inductance L_p is connected in parallel with a smaller loop with self-inductance L_s that serves as the body of the SQUID.

The helium ion direct write SQUID fabricated in this prior work, [15] had an optimum temperature of operation of 10 K. In this manuscript, we fabricate and test a high- $T_{\rm C}$ nano-slit sensor for operation near $T=T_{\rm C}/2$. This temperature was chosen to ensure that the energy gap of the superconductor [19] was fully open to maximize $I_{\rm C}R$, minimize kinetic inductance and reduce changes in parameters from temperature fluctuations. While this is lower than the more common 77 K temperature targeted by others, we feel the gain in performance outweighs the additional power required for cooling.

II. EXPERIMENT

The design of our micro-magnetometer utilizes a 100 μ m diameter pick-up loop connected in parallel with a smaller loop that serves as the body of the SQUID as shown in previously reported work [15]. To increase the temperature of operation to 42 K, the width of the Josephson junctions were increased to 2 μ m and the irradiation dose was reduced by about 25%. The electrical schematic of our sensor design is shown in Fig. 1. Flux penetrating the large loop induces a current that flows through a common electrode shared with the SQUID, thereby coupling additional flux into it. This additional flux concentration significantly increases the sensitivity.

To fabricate nano-slit SQUIDs a commercial 30-nm thick YBCO thin film grown by reactive coevaporation was procured from Ceraco GmbH. Electrodes for electrical contacts and pick-up loops were patterned with photolithography and argon ion milling. Samples were loaded into a Zeiss Orion Plus HIM operating at 32 kV and lines for the Josephson junctions and smaller SQUID loop were irradiated with a dose of 10^{16} He⁺/cm². A detailed description of this process has been published elsewhere [15].

Completed magnetometers were cooled in a liquid helium cryostat, shielded with 3 layers of μ -metal for electrical characterization. The current-voltage characteristic (*I-V*) was measured and is shown in Fig. 2(a). The critical current and resistance were 15 μ A and 5 Ω respectively at 42 K. The voltage-magnetic field characteristic (*V-B*) (Fig. 2(c)) reveals a modulation of \sim 20 μ V

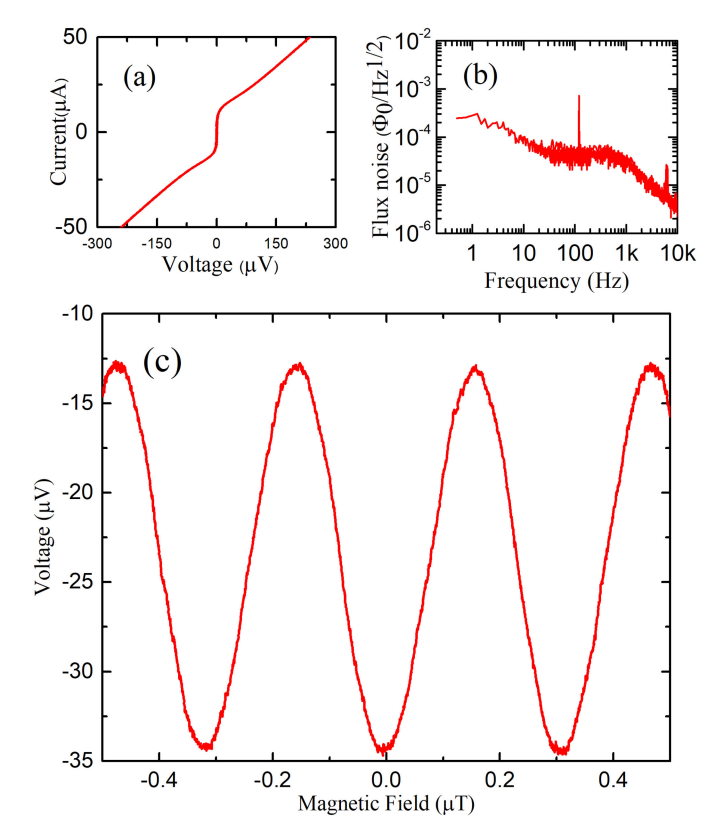


Fig. 2. (a) Current - Voltage characteristic of the magnetometer, the critical current and resistance are 15 μA and 5 Ω respectively at 42 K; (b) flux noise of the SQUID measured at 42 K; (c) Voltage-Magnetic field characteristic of the magnetometer, the SQUID oscillation reveals a modulation of ${\sim}20~\mu V$ and period of ${\sim}300~\mu T/\Phi_0$ at 42 K.

and period of ${\sim}300~\text{nT/}\Phi_0$ at 42 K. The flux noise of the SQUID (Fig. 2(b)) was found to be around $5\times10^{-5}~\Phi_0/\text{Hz}^{1/2}$ with a field sensitivity of about 15 pT/Hz $^{1/2}$.

Magnetic Fe $_3$ O $_4$ nanoparticles were imaged in a scanning electron microscope to determine size and uniformity. As seen in Fig. 3 the particles were about 75 nm \pm 5 nm in diameter. Magnetization as a function of applied field was measured in a Quantum Design MPMS3 at room temperature, as shown in Fig. 3 (inset). Based on the work done by Goya *et al.* [20], the ratio of remanence and saturation magnetization for 50 nm Fe $_3$ O $_4$ nanoparticles were 0.21 and 0.15 at 5 K and 300 K respectively, so we expect only a small change in properties upon cooling. With the initial electrical characterization complete, we conducted an experimental estimate of the sensitivity of the nano-slit magnetometer to magnetic nanoparticles. The saturation magnetization occurred near 200 Oe with a magnetic moment of around 0.0002 emu.

The SQUID was covered by a layer of epoxy, with an estimated thickness of 1 mm, then a small droplet of nanoparticles was placed directly on top of the epoxy and air dried before cooling and re-measurement of V-B characteristics. Fig. 4 shows several periods of V-B curve before and after application of the nanoparticles. The SQUID is shifted by around 30 periods corresponding to a value of of 10 μ T, evidenced by the shift of the Fraunhofer envelope of the critical current.

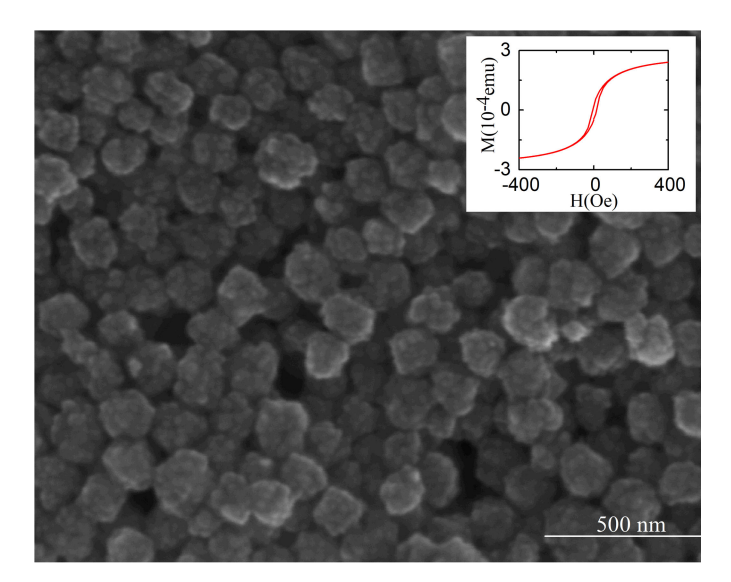


Fig. 3. SEM image of the Fe $_3$ O₄ nanoparticles, the diameter of these nanoparticles is about 75 nm \pm 5 nm; inset figure is the field dependence of moment for the Fe $_3$ O₄ nanoparticles measured in a Quantum Design MPMS3 at room temperature, the saturation magnetization occurred near 200 Oe with a magnetic moment of around 2×10^{-4} emu.

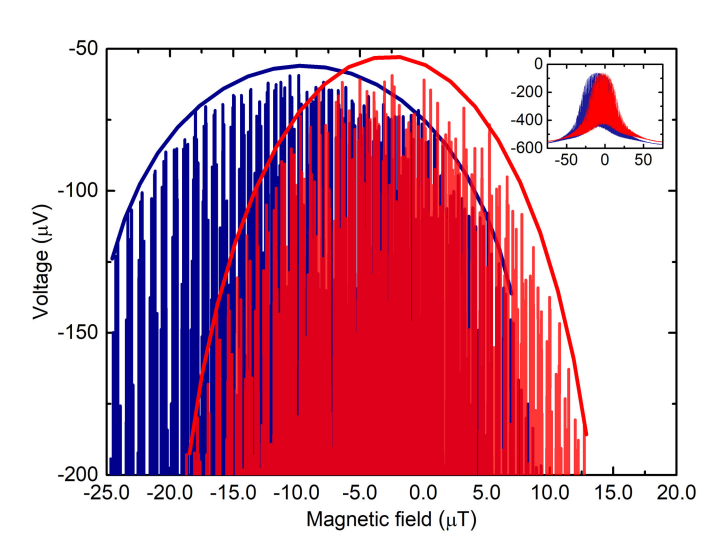


Fig. 4. Voltage - Magnetic field characteristics of the SQUID before and after application of Fe $_3$ O $_4$ nanoparticles at 42 K, the red and blue pattern show the Fraunhofer pattern before and after application of nanoparticles respectively, the inset figure shows a large range of Fraunhofer pattern.

III. DISCUSSION

The nanoparticles cover a round area of around $100~\mu m$ in diameter, the ratio of distance between the SQUID and nanoparticles to the diameter of area covered by nanoparticles is around 10. Therefore we assume the nanoparticles behaved as a single magnetic dipole and can be described by the following equation:

$$\vec{B}(\vec{r}) = \frac{\mu_0}{4\pi} \frac{|\vec{m}|}{|\vec{r}|^3} (2\cos\theta \hat{r} + \sin\theta \hat{\theta})$$
 (1)

Where \vec{B} is magnetic flux density in Tesla, μ_0 is the vacuum permeability, \vec{m} is the magnetic moment, \vec{r} is the distance between the nanoparticles and the SQUID, θ is the polar angle, \hat{r} is the unit radial vector, and $\hat{\theta}$ is the unit polar angle vector in spherical coordinates with the magnetic moment aligned with the z-axis.

In Fig. 4, a 10 μ T magnetic field is detected, according to eq. 1, assuming θ to be 0 degree, the magnetic moment of the nanoparticles is 5×10^{-5} emu, which is consistent with the measurement in Fig. 3 (inset) (2.5×10^{-5}) emu at 0.1 Oe). The factor of two difference is reasonable due to the uncertainty in our estimate of the epoxy thickness and the temperature difference of the two measurements. The number density of the Fe₃ O₄ nanoparticles is estimated to be 80 μ m² based on the image in Fig. 3. The area covered by nanoparticles is around 8,000 μ m², which suggests 64,000 Fe₃ O₄ nanoparticles were immobilized on the SQUID magnetometer. However based on the field sensitivity of this SQUID, the minimum number of nanoparticles required for detection with this SQUID at 1 mm is less than 1500. If completely magnetized prior to measurement with a large saturation field we predict a detection capability of just 150 nanoparticles.

IV. CONCLUSION

This work was the first step to building a helium ion beam fabricated nano-slit SQUID based micro-magnetometer detection system for biological specimens. Future work will be to package this magnetometer onto a small single stage cryocooler equipped with a narrow vacuum jacketed window for detection of samples at room temperature. We find the large deflection of the Fraunhoffer pattern an encouraging result considering that we will need to perform detection at larger distances for this task. The ability of the helium ion beam patterning technique to precisely tune SQUID properties may open up many new applications for high- $T_{\rm C}$ SQUIDs.

ACKNOWLEDGMENT

The authors thank Xiaoping Hu, Kaiqing Chen, and Yaocai Bai for synthesis of the Fe_3O_4 nanoparticles used in this work. The authors thank Shozo Yoshizumi for providing susceptibility measurements of the Fe_3O_4 nanoparticles used in this work.

REFERENCES

- A. S. Arbab, L. A. Bashaw, B. R. Miller, E. K. Jordan, J. W. Bulte, and J. A. Frank, "Intracytoplasmic tagging of cells with ferumoxides and transfection agent for cellular magnetic resonance imaging after cell transplantation: Methods and techniques," *Transplantation*, vol. 76, no. 7, pp. 1123–1130, 2003.
- [2] M. Lewin et al., "Tat peptide-derivatized magnetic nanoparticles allow in vivo tracking and recovery of progenitor cells," Nat. Biotechnol., vol. 18, no. 4, pp. 410–414, 2000.
- [3] J.-J. Lin et al., "Folic acid–pluronic F127 magnetic nanoparticle clusters for combined targeting, diagnosis, and therapy applications," *Biomaterials*, vol. 30, no. 28, pp. 5114–5124, 2009.
- [4] F. Ludwig, E. Heim, D. Menzel, and M. Schilling, "Investigation of superparamagnetic Fe₃ O₄ nanoparticles by fluxgate magnetorelaxometry for use in magnetic relaxation immunoassays," *J. Appl. Phys.*, vol. 99, no. 8, pp. 08P106-1–08P106-3, 2006.

- [5] M. Faley et al., "High-T_c SQUIDs biomagnetometers," Supercond. Sci. Technol., vol. 30, no. 8, 2017, Art. no. 083001.
- [6] S. Sepehri et al., "Volume-amplified magnetic bioassay integrated with microfluidic sample handling and high-T_c SQUIDs magnetic readout," APL Bioengineering, vol. 2, no. 1, 2018, Art. no. 016102.
- [7] P. C. Chu, "High-temperature superconductors," Sci. Am., vol. 273, no. 3, pp. 162–165, 1995.
- [8] T. Scherer, P. Marienhoff, R. Herwig, M. Neuhaus, and W. Jutzi, "Anisotropy on the a, b-plane of c-axis orientated almost twin-free YBCO films on NdGaO₃," *Physica C*, vol. 197, no. 1–2, pp. 79–83, 1992.
- [9] H. Jiang, T. Yuan, H. How, A. Widom, C. Vittoria, and A. Drehman, "Measurements of anisotropic characteristic lengths in YBCO films at microwave frequencies," *J. Appl. Phys.*, vol. 73, no. 10, pp. 5865–5867, 1993.
- [10] M. Faley, U. Poppe, K. Urban, D. Paulson, and R. Fagaly, "A new generation of the HTS multilayer DC-SQUID magnetometers and gradiometers," J. Phys. Conf. Ser., vol. 43, no. 1. IOP Publishing, 2006, p. 1199.
- [11] S. Adachi et al., "Preparation of multilayer films for integrated high-T_c SQUIDs with ramp-edge Josephson junctions," *Physica C*, vol. 468, no. 15–20, pp. 1936–1941, 2008.
- [12] C. Foley et al., "New techniques for fabricating step-edge junctions for high-T_c SQUIDs on MgO substrates," *IEEE Trans. Appl. Supercond.*, vol. 3, no. 1, pp. 2361–2364, Mar. 1993.
- [13] E. Y. Cho et al., "YBa₂Cu₃O_{7-δ} superconducting quantum interference devices with metallic to insulating barriers written with a focused helium ion beam," Appl. Phys. Lett., vol. 106, no. 25, 2015, Art. no. 252601.

- [14] M. Chukharkin et al., "Improvement of ultra-low field magnetic resonance recordings with a multilayer flux-transformer-based high-tc squid magnetometer," *IEEE Trans. Appl. Supercond*, vol. 23, no. 3, Jun. 2013, Art. no. 1602704.
- [15] E. Y. Cho, H. Li, J. C. Lefebvre, Y. W. Zhou, R. Dynes, and S. A. Cybart, "Direct-coupled micro-magnetometer with Y–B–Cu–O nano-slit squid fabricated with a focused helium ion beam," *Appl. Phys. Lett.*, vol. 113, no. 14, Oct. 2018. [Online]. Available: http://par.nsf.gov/biblio/10076662
- [16] B. Ward, J. A. Notte, and N. Economou, "Helium ion microscope: A new tool for nanoscale microscopy and metrology," *J. Vac. Sci. Technol.*, vol. 24, no. 6, pp. 2871–2874, 2006.
- [17] E. Y. Cho, Y. W. Zhou, J. Y. Cho, and S. A. Cybart, "Superconducting nano Josephson junctions patterned with a focused helium ion beam," *Appl. Phys. Lett.*, vol. 113, no. 2, 2018, Art. no. 022604.
- [18] S. A. Cybart et al., "Temporal stability of Y–B–Cu–O nano Josephson junctions from ion irradiation," *IEEE Trans. Appl. Supercond*, vol. 23, no. 3, Jun. 2013, Art. no. 1100103.
- [19] S. A. Cybart *et al.*, "Nano Josephson superconducting tunnel junctions in YBa₂Cu₃O_{7- δ} directly patterned with a focused helium ion beam," *Nat. Nanotechnol.*, vol. 10, no. 7, pp. 598–602, 2015.
- [20] G. Goya, T. Berquo, F. Fonseca, and M. Morales, "Static and dynamic magnetic properties of spherical magnetite nanoparticles," *J. Appl. Phys.*, vol. 94, no. 5, pp. 3520–3528, 2003.